INTERNATIONAL JOURNAL FOR NUMERICAL METHODS IN FLUIDS
Int. J. Numer. Meth. Fluids 2009; **60**:1–26
Published online 18 July 2008 in Wiley InterScience (www.interscience.wiley.com). DOI: 10.1002/fld.1875

Assessment of a high-order finite difference upwind scheme for the simulation of convection–diffusion problems

V. G. Ferreira[1,*,†], F. A. Kurokawa[1], R. A. B. Queiroz[1], M. K. Kaibara[2], C. M. Oishi[1], J. A. Cuminato[1], A. Castelo[1], M. F. Tomé[1] and S. McKee[3]

[1]*Departamento de Matemática Aplicada e Estatística, Instituto de Ciências Matemáticas e de Computação-USP, Av. Trabalhador São Carlense, 400, C.P. 668, 13560-970 São Carlos, SP, Brazil*
[2]*Departamento de Matemática, Faculdade de Ciências, Unesp, Bauru, SP, Brazil*
[3]*Department of Mathematics, University of Strathclyde, Glasgow, U.K.*

SUMMARY

This article deals with the study of the development and application of the high-order upwind ADBQUICKEST scheme, an adaptative bounded version of the QUICKEST for unsteady problems (*Commun. Numer. Meth. Engng* 2007; **23**:419–445), employing both linear and nonlinear convection term discretization. This scheme is applicable to a wide range of computational fluid dynamics problems, where transport phenomena are of special importance. In particular, the performance of the scheme is assessed through an extensive numerical simulation study of advection–diffusion problems. The scheme, implemented in the context of finite difference methodology, combines a good approximation of shocks (or discontinuities) with a good approximation of the smooth parts of the solutions. In order to assess the performance of the scheme, seven problems are solved, namely (a) advection of scalars; (b) non-linear viscous Burgers equation; (c) Euler equations of gas dynamics; (d) Newtonian flow in a channel; (e) axisymmetric Newtonian jet flow; (f) axisymmetric non-Newtonian (generalized Newtonian) flow in a pipe; and (g) collapse of a fluid column. The numerical experiments clearly show that the scheme provides more consistent solutions than those found in the literature. From the study, the flexibility and robustness of the ADBQUICKEST scheme is confirmed by demonstrating its capability to solve a variety of linear and nonlinear problems with and without discontinuous solutions. Copyright © 2008 John Wiley & Sons, Ltd.

Received 25 October 2007; Revised 10 April 2008; Accepted 2 June 2008

KEY WORDS: high-order upwind schemes; convective terms; numerical simulation; finite differences; advection–diffusion equations

*Correspondence to: V. G. Ferreira, Departamento de Matemática Aplicada e Estatística, Instituto de Ciências Matemáticas e de Computação-USP, Av. Trabalhador São Carlense, 400, C.P. 668, 13560-970 São Carlos, SP, Brazil.
†E-mail: pvgf@icmc.usp.br

Contract/grant sponsor: FAPESP; contract/grant numbers: 03/12612-9, 04/16064-9, 05/51458-0, 06/05910-1
Contract/grant sponsor: CNPq; contract/grant numbers: 304201/2005-7, 472030/2006-0

1. INTRODUCTION

The development of upwind differencing schemes for approximating linear or non-linear convective terms in advection–diffusion equations has been a subject of concern for more than three decades. In the case of the hydrodynamic flow equations (see, e.g. [1]), the classical one-sided first-order upwind (donor cell low-order) and Lax–Friedrichs finite difference schemes [2–4] can generate significant errors; the most serious is the production of a diffusive effect (numerical false diffusion [5, 6]) that augments the effects of viscosity. On the other hand, standard second- or higher-order difference schemes, such as central difference (CD), second-order upwind (SOU) [7], quadratic upstream interpolation for convective kinematics (QUICK) [8] and Lax–Wendroff [9], have been popular techniques for approximating these non-linear advection terms. However, the use of these schemes in the proximity of discontinuities typically introduces dispersive effects that lead to non-physical, spurious oscillations (numerical oscillations) that corrupt the solution and lead to numerical instability [3, 10]. As a consequence, this has led to the development of sophisticated high-order finite difference upwind schemes for the simulation of convection–diffusion problems.

The oscillatory behavior of the numerical solution around the discontinuities and extremal points can be prevented by using more sophisticated high-order upwind schemes that have the following attractive properties: (i) they are at least second-order accurate in regions where the solution is smooth; (ii) they have a monotonic behavior near the discontinuities (boundedness); (iii) they do not spread the solution by introducing too much numerical false diffusion, (iv) they do not need artificial viscosity; (v) they take into account the propagation of physical information ('wind' or 'wave' direction); and (vi) they incorporate the one-sided first-order upwind scheme in their formulation (avoidance of wiggling). Representative examples of schemes that attempt to meet these requirements are variable-order non-oscillatory scheme (VONOS) [11], hybrid-linear parabolic approximation (HLPA) [12], sharp and monotonic algorithm for realistic transport (SMART) [13], weighted-average coefficient ensuring boundedness (WACEB) [14], convergent and universally bounded interpolation scheme for the treatment of advection (CUBISTA) [15] and, more recently, our adaptative bounded version of the QUICK with estimated streaming terms (QUICKEST) [16], called here ADBQUICKEST, the object of this study.

In this paper, the effectiveness of the ADBQUICKEST scheme has been evaluated by means of seven distinct test cases. These are (a) advection of scalars; (b) one-dimensional (1D) non-linear viscous Burgers equation; (c) 1D Euler equations of gas dynamics; (d) 2D Newtonian flow in a channel; (e) axisymmetric Newtonian jet flow; (f) axisymmetric generalized Newtonian flow in a pipe, and (g) 2D/3D collapse of a fluid column. The numerical results were compared with analytic and experimental results, and/or very accurately computed numerical results.

This study has two specific objectives: the first is to highlight the ADBQUICKEST scheme as an effective new methodology for solving advection–diffusion problems and the second is to extend the applicability of the previous results [16, 17] to problems that are sufficiently difficult and wide-ranging.

The organization of this study is as follows. In Section 2, the ADBQUICKEST scheme used in our numerical calculations is described. In Section 3, some numerical test problems and their numerical solutions are presented. Section 4 contains our conclusions and discusses the future direction of this work.

DOI: 10.1002/fld

2. DESCRIPTION OF THE ADBQUICKEST SCHEME

Consider the 1D advection of a scalar

$$\begin{aligned} &\frac{\partial u}{\partial t}+a\frac{\partial u}{\partial x}=0 \quad \text{with } a=\text{const.}>0 \\ &u(x,0)=u_0(x), \quad x\in\mathbb{R} \end{aligned} \tag{1}$$

together with appropriate periodic boundary conditions. The solution of this equation ($u(x,t)=u_0(x-at)$) is approximated by the conservative finite difference method

$$u_i^{n+1}=u_i^n-\theta(u_{i+1/2}^n-u_{i-1/2}^n) \tag{2}$$

where u_i^n is the numerical solution at point $(i\delta_x, n\delta_t)$ and $\theta=a\delta_t/\delta_x$ is the Courant or Courant–Friedrich–Levy (CFL) number. In the above equation, $u_{i+1/2}^n$ and $u_{i-1/2}^n$ are the interface numerical fluxes, depending on values at three selected points, and are denoted, respectively, by u_f and u_g (see Figure 1). For example, in Figure 1, the f face, together with its convection velocity $V_f>0$ and neighboring nodes D, U and R, is presented. The variation of a convected property u through, for example, the boundary face f between two control volumes can be represented by a functional relationship linking values u_{D}, u_{U} and u_{R}, which represent, respectively, the downstream, the upstream and the remote-upstream locations with respect to the convecting velocity V_f at the interface f (see Figure 1). The same treatment is given by g face. If this functional relationship involving these three positions is prescribed, then the interface numerical flux value can be determined. To this end, the original variable u is transformed into the normalized variable of Leonard [18] by

$$\hat{u}(x,t)=\frac{u(x,t)-u_{\mathrm{R}}^n}{u_{\mathrm{D}}^n-u_{\mathrm{R}}^n}$$

The advantage of this normalization is that the interface value $\hat{u}_f$ depends on $\hat{u}_{\mathrm{U}}^n$ and θ only, since $\hat{u}_{\mathrm{D}}^n=1$ and $\hat{u}_{\mathrm{R}}^n=0$.

The choice of interface fluxes in Equation (2) determines the particular upwinding scheme for Equation (1). In this study, these fluxes will be approximated by the ADBQUICKEST scheme [16] (see also [17], where it appeared for the first time). This scheme can be regarded as a convective interpolation technique for transient equations. Although there is no shock formation in Newtonian incompressible fluids, this scheme has been found to be effective in 2D computations (see [16]). The ADBQUICKEST scheme was proposed in the context of the normalized variable formulation (NVF) of Leonard and Niknafs [19] while enforcing the total-variation diminishing (TVD) property (i.e. the norm of gradients of a field cannot be increased by the scheme [20])

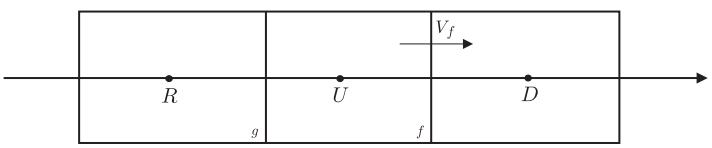

Figure 1. Neighboring nodes D, U and R of the f face.

DOI: 10.1002/fld

of Harten [21] and Sweby [22]. Consequently, it satisfies the convection boundedness criterion (CBC) of Gaskell and Lau [13]. The main idea in the derivation of this scheme was to combine accuracy and monotonicity, while ensuring flexibility. It can also ensure that the total variation of the variables does not increase with time; thus, no spurious numerical oscillations (maxima or minima) are generated. The numerical solution obtained with this scheme can be second- or third-order accurate in the smooth parts of the solution domain, but only first-order near regions with large gradients (shock, contact surface).

In summary, the functional relationship of the ADBQUICKEST scheme and its corresponding flux limiter are as follows:

$$\hat{u}_f = \begin{cases} (2-\theta)\hat{u}_U, & 0<\hat{u}_U<a \\ \hat{u}_U+\frac{1}{2}(1-\theta)(1-\hat{u}_U)-\frac{1}{6}(1-\theta^2)(1-2\hat{u}_U), & a\leqslant\hat{u}_U\leqslant b \\ 1-\theta+\theta\hat{u}_U, & b<\hat{u}_U<1 \\ \hat{u}_U & \text{elsewhere} \end{cases} \tag{3}$$

The constants a and b in Equation (3) are given by

$$a=\frac{2-3\theta+\theta^2}{7-9\theta+2\theta^2} \quad \text{and} \quad b=\frac{-4+3\theta+\theta^2}{-5+3\theta+2\theta^2}$$

Figure 2 shows the ADBQUICKEST scheme in the normalized variable diagram ($\hat{u}_U-\hat{u}_f$ plane). The corresponding flux limited function for the ADBQUICKEST scheme is derived as follow.

First, Equation (3) is written in terms of the normalized variable as

$$\hat{u}_f=\hat{u}_U+\tfrac{1}{2}\psi(r_f)(1-\hat{u}_U) \tag{4}$$

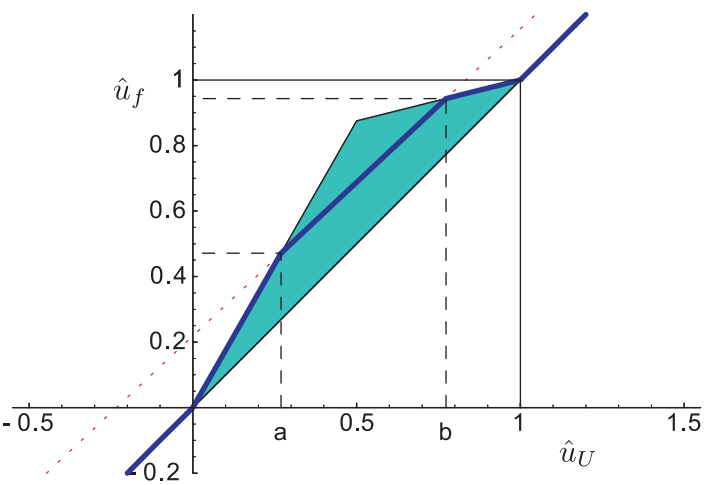

Figure 2. A graph of the normalized variable of $\hat{u}_f$ for QUICKEST scheme (dotted) and ADBQUICKEST scheme with $\theta=0.5$ (solid).

DOI: 10.1002/fld

In terms of the unnormalized variable, Equation (4) can be written as

$$u_f = u_U + \tfrac{1}{2}\psi(r_f)(u_D - u_U) \tag{5}$$

where ψ is the so-called flux limiter that determines the level of antidiffusive flux, and r_f (a sensor) is the ratio of upstream to downstream (consecutive) gradients

$$r_f = \frac{(\partial u/\partial x)_g}{(\partial u/\partial x)_f} \tag{6}$$

which for uniform meshes can be rewritten as

$$r_f = \frac{u_U - u_R}{u_D - u_U} \tag{7}$$

In terms of the normalized variable, this ratio can be expressed as

$$r_f = \frac{\hat{u}_U}{1 - \hat{u}_U} \tag{8}$$

From Equations (3), (4), and (8), we deduce the flux limiter for the QUICKEST adaptative scheme

$$\psi(r_f) = \begin{cases} 2r_f, & 0 < r_f < p \\ \dfrac{2+\theta^2-3\theta+(1-\theta^2)r_f}{3-3\theta}, & p \leqslant r_f \leqslant q \\ 2, & r_f > q \\ 0, & r_f < 0 \end{cases} \tag{9}$$

where

$$p = \frac{\theta-2}{\theta-5} \quad \text{and} \quad q = \frac{\theta+4}{\theta+1}$$

According to Equations (5) and (9), the ADBQUICKEST is adaptative in the sense that flux approximation is set depending on the smoothness of the solution.

The flux limiter (9) can be also written, in a more widely used notation (see, e.g. [20]), as

$$\psi(r_f) = \max\left\{0, \min\left[2r_f, \frac{2+\theta^2-3\theta+(1-\theta^2)r_f}{3-3\theta}, 2\right]\right\}$$

Within the Sweby TVD region, the plot of the flux limiter (9), for several values of θ, is presented in Figure 3. Note that for all values of the parameter θ, the flux limiter passes through the point $(1, 1)$ in the TVD region, which is the necessary and sufficient condition for second-order accuracy away from extrema (see [22]) and corresponds to point $(0.5, 0.75–0.25\theta)$ in the NVD of Leonard [18] (see CBC region in [13, 20]). One can note that when the parameter θ tends to 0, the flux (3) passes through the point $(0.5, 0.75)$ in the NVD region, which is the necessary and sufficient condition for second-order accuracy and corresponds to point $(1, 1)$ in the Sweby TVD region.

DOI: 10.1002/fld

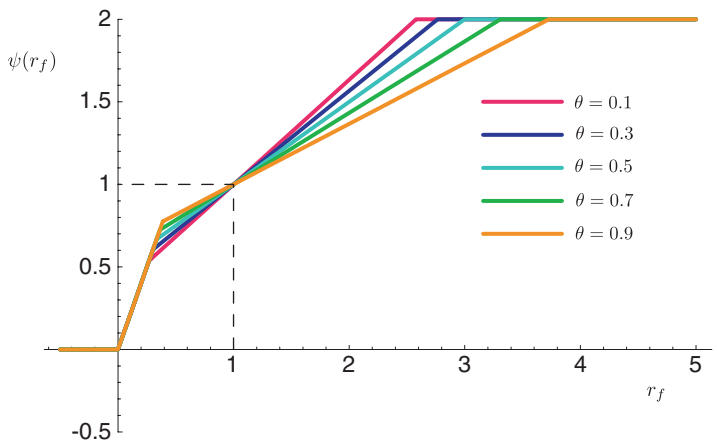

Figure 3. Flux limiter of the ADBQUICKEST scheme in the Sweby TVD region for several values of Courant number θ.

3. NUMERICAL TEST PROBLEMS

In this section, some numerical tests are performed to demonstrate the flexibility and robustness of the ADBQUICKEST scheme described in the previous section.

The ADBQUICKEST scheme has the advantage of being a bounded version of the QUICKEST. Besides, an important issue in using this technique is the intrinsic nature of the Courant number θ, which gives flexibility to users. In the simulation of 1D problems with or without discontinuities, smaller Courant numbers are usually used, typically in the range of 0.5–0.8. In the simulation of 2D and 3D fluid flow problems, the Courant number is automatically set by the numerical procedures, that is, this parameter is calculated according to the local flow without need of action taken from the user.

All the computations to follow were carried out with the aid of a PC computer with AMD Athlon 64 X2 2.22 GHz processor available at the High Performance Computing Laboratory (LCAD) of the Institute of Mathematics and Computer Sciences—University of São Paulo (ICMC-USP). We first solve the problem of advection of scalars. We then consider the 1D viscous Burgers equation and shock tube problems. Following on from these, we solve the full 2D and axisymmetric Navier–Stokes equations describing the flow of an incompressible Newtonian (or generalized Newtonian) fluid. Finally, we performed direct numerical simulations of the collapse of fluid columns. These problems appear frequently in fluid dynamics studies and are described/simulated in the following subsections.

For simplicity, for all calculations we used first-order Euler forward differences for temporal discretization, except for the fully developed flow in a channel at $Re = 500$ described in Section 3.4.1, where we used the Crank–Nicolson implicit method.

3.1. Linear advection equation

One of the simplest hyperbolic systems arising from the conservation laws is the scalar linear advection equation (1), describing the advection or transport of the quantity u along the x-axis with

DOI: 10.1002/fld

uniform velocity $a=1$. This equation is supplemented with the four initial conditions presented in the following tests.

3.1.1. Non-smooth initial distribution (see [23]). In this first test case, on the domain $[-1, 1]$, we solve (1) with u_0 given by

$$u_0(x)=\begin{cases} -x\sin\left(\dfrac{3\pi x^2}{2}\right), & -1\leqslant x\leqslant -\dfrac{1}{3} \\ |\sin(2\pi x)|, & |x|<\frac{1}{3} \\ 2x-1-\frac{1}{6}\sin(3\pi x), & \frac{1}{3}\leqslant x\leqslant 1 \end{cases} \tag{10}$$

This problem was run on a grid of 200 computational cells with a Courant number of 0.8 and until a final time of $t=1.0$. Figure 4 presents the exact solution and the numerical results. One can clearly observe from this figure that the ADBQUICKEST scheme produces accurate results over the whole domain, capturing the shocks very well indeed.

Figure 5 presents the solution errors, using a Courant number of 0.8 and final time of $t=1.0$ for all cases, in several norms for different mesh sizes. It can also be observed that, for this highly discontinuous problem, the order of the accuracy of the ADBQUICKEST scheme is, as expected, only around unity (due to sharp fronts of the advected variable). This observation is in good overall agreement with those obtained by Titarev and Toro [24].

3.1.2. Smooth initial distribution (see [25]). This test is used to compare the ADBQUICKEST, with the well-known CUBISTA [15], WACEB [14] and SMART [13] schemes, applied to Equation (1), on the domain $[-\pi, \pi]$, with $u_0(x)=\sin(\pi x)$. Using these four bounded upwind schemes, the numerical solutions are carried out with increasing resolution up to a mesh of 320 cells. We have

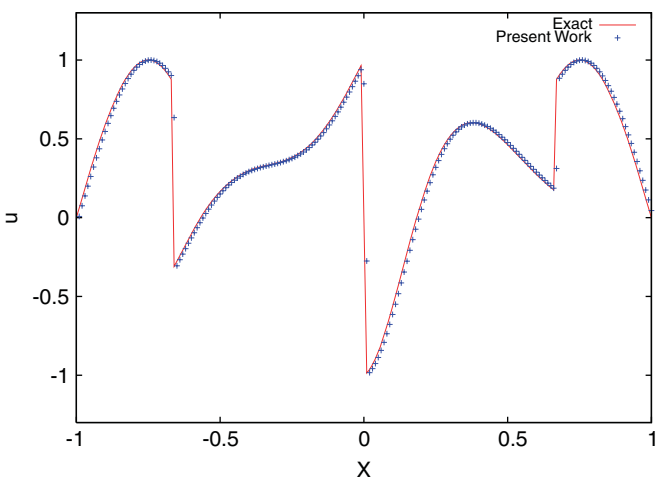

Figure 4. Computed (present work) solution with 200 cells and analytic (exact) solution for the linear advection equation using the initial data (10).

DOI: 10.1002/fld

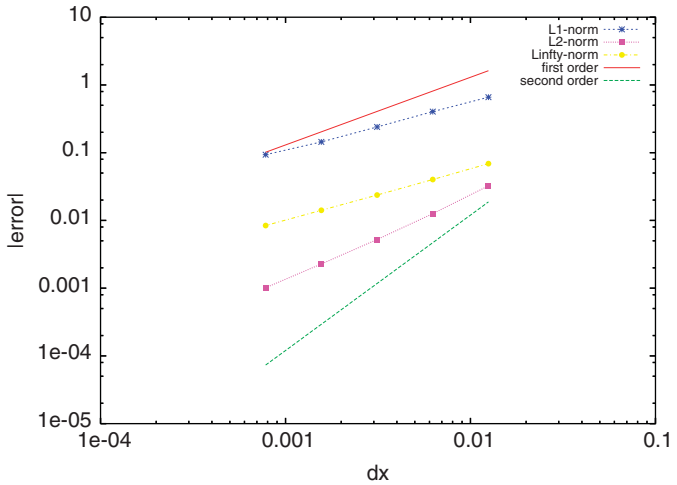

Figure 5. The error in the solution of linear advection equation (1) and (10).

Table I. Convergence test: L_1, L_2 and L_∞ errors and convergence-order estimates for several schemes using $u(x,0)=\sin(x)$, $-\pi\leqslant x\leqslant\pi$.

Scheme	N	L_1 error	L_1 order	L_2 error	L_2 order	L_∞ error	L_∞ order
ADBQUICKEST	20	0.2736e−1	—	0.3182e−1	—	0.5287e−1	—
	40	0.7997e−2	1.775	0.1121e−1	1.505	0.2580e−1	1.092
	80	0.2521e−2	1.665	0.4532e−2	1.306	0.1200e−1	1.047
	160	0.7952e−3	1.664	0.1821e−2	1.315	0.6231e−2	0.945
	320	0.2467e−3	1.688	0.7394e−3	1.300	0.2920e−2	1.093
CUBISTA	20	0.3728e−1	—	0.4109e−1	—	0.6456e−1	—
	40	0.1151e−1	1.695	0.1539e−1	1.417	0.3321e−1	0.937
	80	0.3877e−2	1.582	0.6464e−2	1.250	0.1804e−1	0.880
	160	0.1233e−2	1.652	0.2599e−2	1.314	0.9092e−2	0.988
	320	0.4903e−3	1.688	0.1999e−2	1.241	0.4460e−2	1.027
WACEB	20	0.2855e−1	—	0.3198e−1	—	0.5016e−1	—
	40	0.8756e−2	1.705	0.1139e−1	1.489	0.2287e−1	1.133
	80	0.2762e−2	1.665	0.4318e−2	1.402	0.1250e−1	0.871
	160	0.8811e−3	1.648	0.1663e−2	1.377	0.7031e−2	0.830
	320	0.2852e−3	1.627	0.7534e−3	1.142	0.3650e−2	0.946
SMART	20	0.1678e−1	—	0.2070e−1	—	0.6662e−1	—
	40	0.6516e−2	1.365	0.1027e−1	1.021	0.3493e−1	0.931
	80	0.2368e−2	1.460	0.4544e−2	1.176	0.1655e−1	1.078
	160	0.8069e−3	1.553	0.1758e−2	1.370	0.9482e−2	0.804
	320	0.3050e−3	1.403	0.7621e−3	1.205	0.4990e−2	0.926

shown in Table I the L_1, L_2 and L_∞ error norms, as well as the accuracy estimates, of the computed solutions using $\theta=0.5$. From this table, the numerical data indicate that, on these norms, the ADBQUICKEST scheme converges at a rate higher than that of CUBISTA, WACEB and SMART

DOI: 10.1002/fld

schemes. Particularly, it is seen from L_1 error that the ADBQUICKEST shows slightly less than second-order accuracy.

3.1.3. Very flat initial distribution (see [26]*).* Here we presents a similar convergence study to that given in the previous test, with the initial distributions $u_0(x)=\sin^4(\pi x)$. As commented by Balsara and Shu [26], these initial conditions are very flat at each maxima; that is, the first three derivatives are zero there. For this reason, Rogerson and Melburg [27] (see also results obtained with WENO scheme by Herrmann *et al.* [25]) found that ENO-type schemes suffer from a dramatic reduction in accuracy for this case. Table II shows the errors as well as the accuracy estimates for ADBQUICKEST, CUBISTA, WACEB and SMART schemes. One can see from this table that, on L_1 error, the ADBQUICKEST scheme has retained second-order accuracy for this profile. It can also be seen, in comparison with the first test case, the improvement in accuracy from first- to second-order accuracy and the improvement beyond second order of the ADBQUICKEST scheme—in this test, because of lack of severe gradients.

3.1.4. W-shape initial distribution (see [28]*).* In order to test the behavior of the present upwind scheme on a rather stringent problem, we simulated a moving W-shape problem proposed by Wei and Gu [28], i.e. Equation (1) with $a=1$ and the initial condition given by

$$u_0(x)=\begin{cases}1, & 0\leqslant x\leqslant 0.2\\ 4x-\frac{3}{5}, & 0.2<x\leqslant 0.4\\ -4x+\frac{13}{5}, & 0.4<x\leqslant 0.6\\ 1, & 0.6<x\leqslant 0.8\\ 0 & \text{otherwise}\end{cases} \tag{11}$$

This problem has the so-called contact discontinuities [29] that are well known to be difficult to advect [28, 29]. The simulation of this problem is performed on a mesh of 200 computational cells, to a time of $t=1.0$ and with a Courant number of 0.8. The exact solution and the numerical results obtained with the ADBQUICKEST scheme are presented in Figure 6. One can see from this figure that, in general, the peaks in the advected profile are accurately captured by the ADBQUICKEST scheme.

3.2. Viscous Burgers equation

The performance of the ADBQUICKEST scheme is now examined by applying it to the 1D non-linear viscous Burgers equation

$$\frac{\partial u}{\partial t}+\frac{\partial}{\partial x}\left(\frac{u^2}{2}\right)=\nu\frac{\partial^2 u}{\partial x^2},\quad 0\leqslant x\leqslant 1,\ \ t>0 \tag{12}$$

where $u=u(x,t)$ is the dependent variable, resembling the flow velocity in an incompressible fluid and ν is the 'viscosity' coefficient (constant). It is well known that for $\nu>0$, the viscosity term produces smooth solutions and the energy of the system dissipates smoothly. For $\nu\to 0$, discontinuities (shocks) can develop in the solution, even for prescribed smooth initial data.

DOI: 10.1002/fld

Table II. Convergence test: L_1, L_2 and L_∞ errors and convergence-order estimates for several schemes using $u(x,0)=\sin^4(\pi x)$, $-2\leqslant x\leqslant 2$.

Scheme	N	L_1 error	L_1 order	L_2 error	L_2 order	L_∞ error	L_∞ order
ADBQUICKEST	20	2.072e−1	—	2.111e−1	—	2.486e−1	—
	40	4.722e−2	2.133	5.433e−2	1.958	8.409e−2	1.564
	80	1.139e−2	2.052	1.439e−2	1.917	2.994e−2	1.490
	160	2.368e−3	2.266	3.998e−3	1.848	1.057e−2	1.502
	320	5.269e−4	2.168	1.123e−3	1.832	3.744e−3	1.497
CUBISTA	20	2.138e−1	—	2.197e−1	—	2.588e−1	—
	40	5.665e−2	1.916	6.148e−2	1.837	9.408e−2	1.450
	80	1.564e−2	1.857	1.937e−2	1.666	3.597e−2	1.387
	160	4.404e−3	1.828	6.213e−3	1.640	1.384e−2	1.378
	320	1.125e−3	1.968	1.935e−3	1.683	5.247e−3	1.399
WACEB	20	2.097e−1	—	2.144e−1	—	2.525e−1	—
	40	4.539e−2	2.208	5.373e−2	1.996	8.423e−2	1.584
	80	1.212e−2	1.905	1.557e−2	1.787	3.102e−2	1.441
	160	3.257e−3	1.896	4.712e−3	1.724	1.120e−2	1.469
	320	8.725e−4	1.900	1.399e−3	1.752	4.016e−3	1.479
SMART	20	2.036e−1	—	2.105e−1	—	2.412e−1	—
	40	3.832e−2	2.409	4.341e−2	2.278	8.349e−2	1.530
	80	8.293e−3	2.208	9.949e−3	2.125	2.977e−2	1.488
	160	2.104e−3	1.978	2.525e−3	1.978	1.049e−2	1.505
	320	5.859e−4	1.844	7.736e−4	1.706	3.646e−3	1.525

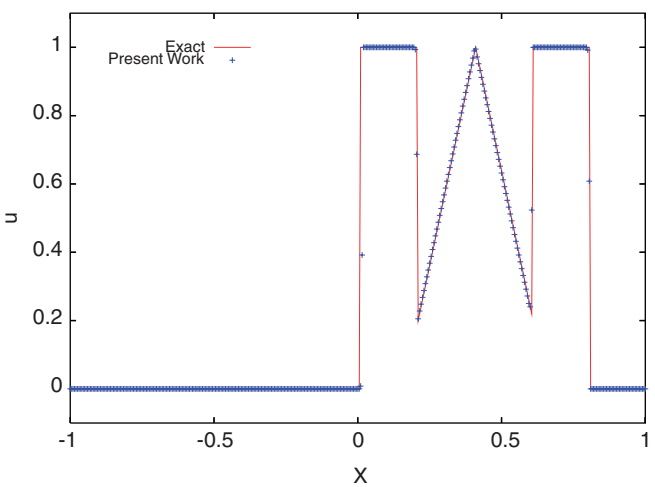

Figure 6. Computed (present work) solution with 200 cells and analytic (exact) solution for the linear advection equation (1) using the initial data (11).

DOI: 10.1002/fld

Burgers equation serves as a good model (combining non-linear advection and linear diffusion) for understanding shock formation and turbulence (see, for instance, [30]). We consider Equation (12) supplemented with the initial condition specified by

$$u(x,0)=\sin(2\pi x)$$

and the boundary conditions

$$u(0,t)=u(1,t)=0$$

In order to numerically solve this initial value problem, a mesh size of 500 computational cells (the method suffers from substantial numerical instability when compared with results on coarser meshes) and a time increment of 0.001 s were used. The ADBQUICKEST scheme was applied with a Courant number of 0.5. Figure 7 displays the performance of the computed solutions using $\nu=0.01$, 0.001, and 0.0001 at five final times $t=0.0, 0.1, 0.2, 0.3, 0.4, 0.5$, given, respectively, the number of time steps (Nt) $0, 100, 200, 300, 400$, and 500. In particular, it can be observed from Figure 7(c) that the formation of a shock appears at $t=0.5$ and that the performance of the ADBQUICKEST scheme in reproducing this discontinuity (without producing spurious oscillations) is very good. Note, also, that the profiles are fully symmetrical about the shock position, which is a desirable feature in a numerical algorithm [26].

3.3. Inviscid Euler equations

In contrast to the preceding test cases, ADBQUICKEST is now applied to more difficult class of problems: hyperbolic systems and in particular shock tube problems resulting in flows with complex structures. The shock tube is an example of a classical 1D compressible flow of an ideal gas and is often used as a test for numerical methods. It consists of a tube filled with gas and separated by a membrane. The state of the gas on the left side of the membrane is different from that on the right (Riemann problem [31]). This results in a discontinuous initial distribution. When the membrane is broken, a complex wave interaction is initiated. The shock tube problem has been used extensively in the literature as a validation test case for high resolution schemes, see, for example, [24, 29, 32] and references therein. The hyperbolic conservation law that models the shock tube problem is the Euler system for 1D gas dynamics, and it takes the form

$$\frac{\partial \mathbf{u}}{\partial t}+\frac{\partial \mathbf{f}(\mathbf{u})}{\partial x}=0 \tag{13}$$

where $\mathbf{u}=(\rho, \rho u, E)^{\mathrm{T}}$ is the vector of conserved variables and $\mathbf{f}(\mathbf{u})$ is the flux function vector $(\rho u, \rho u^2+p, u(E+p))^{\mathrm{T}}$. The variables ρ, u, ρu, E, p are the density, the velocity, the momentum, the total energy and the pressure, respectively. In addition, we require the equation of state for the pressure $p=(\gamma-1)(E-\frac{1}{2}\rho u^2)$, where $\gamma=1.4$ is the ratio of specific heats [23].

3.3.1. Shu–Osher shock tube. The first selected test case, Equation (13) with $-1\leqslant x\leqslant 3$, is the Shu–Osher problem [33], a standard shock/turbulence interaction model that describes an acoustic wave interacting with a sinusoidal density disturbance (see [24, 26, 34, 35]). This problem provides a good test for examining the performance of high-order upwind schemes because it involves a

DOI: 10.1002/fld

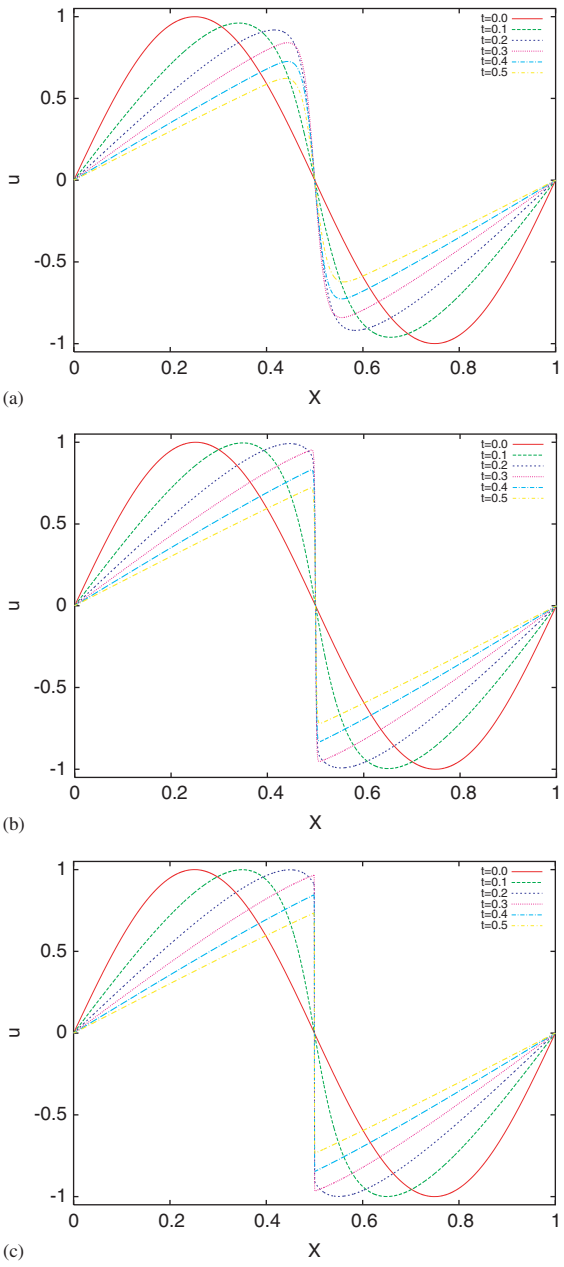

Figure 7. Results for Burgers equation: (a) $\nu = 0.01$; (b) $\nu = 0.001$; and (c) $\nu = 0.0001$.

DOI: 10.1002/fld

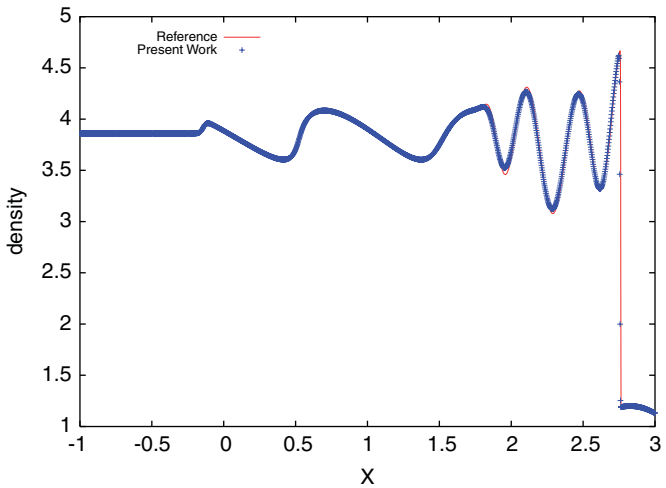

Figure 8. Density distribution for Shu–Osher shock tube problem at $t=1.0$ computed (symbol) with 400 computational cells using the ADBQUICKEST scheme.

combination of smooth profiles and discontinuities and exhibits an amplification of an acoustic wave behind a shock. The distribution is initialized as

$$(\rho, u, p)^{\mathrm{T}} = \begin{cases} (3.86, 2.63, 10.33)^{\mathrm{T}}, & x < -0.8 \\ (1+0.2\sin(5x), 0, 1)^{\mathrm{T}}, & x \geqslant -0.8 \end{cases}$$

This experiment was run by using a uniform mesh of 400 computational cells ($\delta_t = 0.0166$) at a simulation time of $t=1.0$ and for a Courant number of $\theta=0.6$. Depicted in Figure 8 are the reference solution for density (obtained by running the one-sided first-order upwind scheme on a grid consisting of 1600 computational cells) and numerical results (obtained by the ADBQUICKEST scheme). It can be seen from this figure that the numerical solution converged to the reference calculation (the continuous line) and accurately resolved the shock and the waves behind the shock—especially near $x=2.0$. Figure 9 shows a close-up of the reference solution and numerical solution behind the shock. One can see from this figure that the peaks are relatively well resolved (free from oscillations) by the ADBQUICKEST scheme. It is interesting to note that the numerical results obtained here were comparable to the solution reported by Yang [32] using 400 cells (the same number as the ADBQUICKEST scheme), a Courant number of $\theta=0.8$ and a fourth-order modification of the ENO scheme.

3.3.2. Modified Shu–Osher shock tube. The second problem is a modified shock/turbulence interaction, a variation of the Shu–Osher shock tube problem, proposed by Titarev and Toro [24]. It involves Equation (13) on $-5 \leqslant x \leqslant 5$ with initial conditions given by

$$(\rho, u, p)^{\mathrm{T}} = \begin{cases} (1.515695, 0.523346, 1.80500)^{\mathrm{T}}, & x < -4.5 \\ (1+0.1\sin(20\pi x), 0, 1)^{\mathrm{T}}, & x \geqslant 4.5 \end{cases}$$

DOI: 10.1002/fld

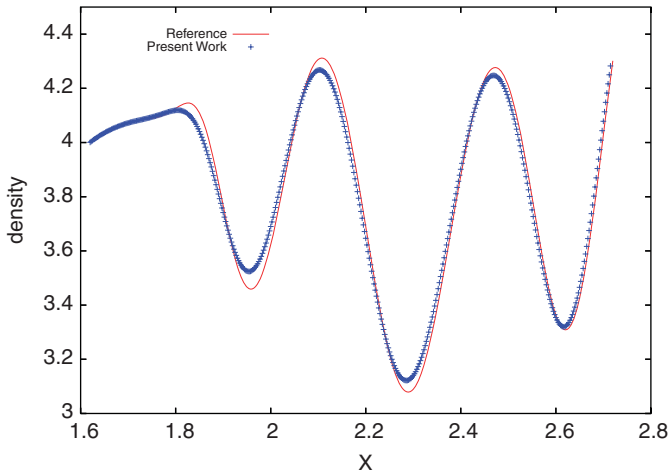

Figure 9. Close-up of the solutions in Figure 8 for $1.6 \leqslant x \leqslant 2.8$.

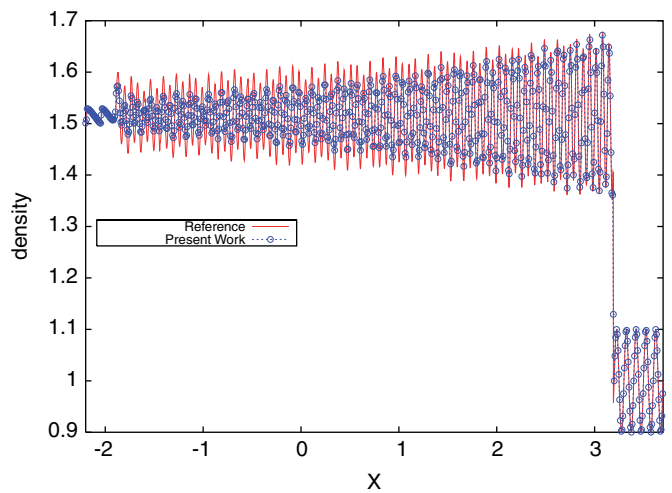

Figure 10. Density distribution for modified Shu–Osher shock tube problem at $t = 5.0$ computed (symbol) with 12 500 computational cells.

Figures 10 and 11 present the reference solution (given by a continuous line and obtained by running the one-sided first-order upwind scheme on a fine grid consisting of 20 000 computational cells) and the numerical results for the density distribution. The numerical results are produced by the ADBQUICKEST scheme on uniform meshes consisting of 12 500 and 18 500 computational cells, at output $t = 5.0$ and for a Courant number of $\theta = 0.2$. For this numerical test, one can see that the ADBQUICKEST scheme on the fine mesh (Figure 11) produces an accurate solution, which is very close to the reference solution.

DOI: 10.1002/fld

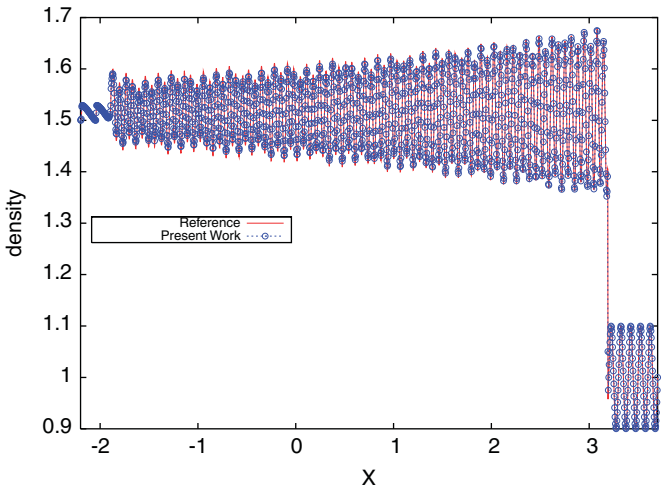

Figure 11. Density distribution for modified Shu–Osher shock tube problem at $t=5.0$ computed (symbol) with 18 500 computational cells.

3.4. 2D and axisymmetric incompressible Navier–Stokes equations

We now assess the performance/applicability of the ADBQUICKEST scheme to solve time-dependent incompressible Navier–Stokes equations. The unsteady flow of an incompressible viscous isothermal Newtonian/non-Newtonian fluid of constant density ρ is modelled by the momentum and continuity equations

$$\frac{\partial u}{\partial t}=-\frac{1}{r^{\alpha}}\frac{\partial(r^{\alpha}uu)}{\partial r}-\frac{\partial(uv)}{\partial z}-\frac{\partial p}{\partial r}+\frac{\eta(q)}{Re}\frac{\partial}{\partial z}\left(\frac{\partial u}{\partial z}-\frac{\partial v}{\partial r}\right)$$
$$+\beta\frac{1}{Re}\left[2\frac{\partial u}{\partial r}\frac{\partial\eta(q)}{\partial r}+\left(\frac{\partial u}{\partial z}+\frac{\partial v}{\partial r}\right)\frac{\partial\eta(q)}{\partial z}\right] \tag{14}$$

$$\frac{\partial v}{\partial t}=-\frac{1}{r^{\alpha}}\frac{\partial(r^{\alpha}uv)}{\partial r}-\frac{\partial(vv)}{\partial z}-\frac{\partial p}{\partial z}-\frac{\eta(q)}{Re}\frac{1}{r^{\alpha}}\frac{\partial}{\partial r}\left(r^{\alpha}\left(\frac{\partial u}{\partial z}-\frac{\partial v}{\partial r}\right)\right)$$
$$+\beta\frac{1}{Re}\left[2\frac{\partial v}{\partial z}\frac{\partial\eta(q)}{\partial z}+\left(\frac{\partial u}{\partial z}+\frac{\partial v}{\partial r}\right)\frac{\partial\eta(q)}{\partial r}\right] \tag{15}$$

$$\frac{1}{r^{\alpha}}\frac{\partial(r^{\alpha}u)}{\partial r}+\frac{\partial v}{\partial z}=0 \tag{16}$$

where t is the time, $u=u(r,z,t)$ and $v=v(r,z,t)$ are, respectively, the components in the r and z directions of the local velocity vector field of the fluid; p is the scalar pressure field divided by the density. The non-dimensional parameter $Re=\rho U_0L_0/\eta$ denotes the associated Reynolds number, in which U_0 is a characteristic velocity scale, L_0 is a length scale, and η is the kinematic molecular viscosity coefficient (constant).

DOI: 10.1002/fld

The parameter α in Equations (14)–(16) is used to specify the coordinate system, namely when $\alpha=0$, plane Cartesian coordinates are considered (r is to be interpreted as x and z as y) and when $\alpha=1$, cylindrical polar coordinates are assumed. The parameter β and the function $\eta(q)$ in Equations (14) and (15) are used to specify Newtonian or non-Newtonian flows: when $\eta(q)=1$ and $\beta=0$, a Newtonian flow with $\eta=\eta_0$ is assumed; when $\beta=1$ and $\eta(q)$ is defined by the cross model (see [36])

$$\eta(q)=\eta_\infty+\frac{\eta_0-\eta_\infty}{1+(Kq)^M} \tag{17}$$

with deformation rate q given by (see [37])

$$q(r,z,t)=\left[2\left(\frac{\partial u}{\partial r}\right)^2+2\left(\frac{\partial v}{\partial z}\right)^2+2\left(\frac{u}{r}\right)^2+\left(\frac{\partial u}{\partial z}+\frac{\partial v}{\partial r}\right)^2\right]^{1/2} \tag{18}$$

a non-Newtonian (to be more precise, a generalized Newtonian) flow is considered. In Equation (17) η_0 and η_∞ (constants) are the asymptotic limits of the viscosity at low ($q\to 0$) and at high ($q\to\infty$) shear rates, respectively. The parameters K and M are positive material constants that determine how the viscosity changes with q between these two asymptotic values (see [37]).

3.4.1. Transient Poiseuille flow. This problem involves the unsteady 2D flow between two parallel stationary infinite plates (channel), placed at $y=0.0\,\mathrm{m}$ and $y=L=1.0\,\mathrm{m}$. The equations that model this problem are (14)–(16) with $\alpha=0$, $\beta=0$, $\eta(q)=1$, $\eta=\eta_0$ and $K=0$ (2D Newtonian case). Initially the fluid is driven by a constant pressure gradient, gradually it flows through the channel and, finally, it arrives at a steady state. The Reynolds number considered here was $Re=0.01$, with the viscosity $\eta=\eta_0=100\,\mathrm{kg/(m\,s)}$ and velocity scale $U_0=1.0\,\mathrm{m/s}$. In order to be able to compare with the analytic solution, the no-slip condition was applied at solid walls. The analytic solution for this flow, obtained by application of Laplace transforms (see [38, 39]), is

$$u(x,y,t)=-4y(y-1)-\frac{32}{\pi^3}\sum_{n=0}^{\infty}(2n+1)^3\sin(\pi y(2n+1))\exp(-Re^{-1}(2n+1)^2\pi^2 t) \tag{19}$$

where x is the coordinate in the streamwise direction and y is the coordinate in the direction normal to the channel. The calculations were carried out using the Freeflow code of Castelo *et al.* [40], which was appropriately modified to incorporate the ADBQUICKEST scheme. At the inlet section, the initial condition was obtained from (19) by setting $t=0$. In the simulation, the computational domain was taken to be $5L\times L$, which was discretized into a 100×20 uniform cells ($\delta_x=\delta_y=0.05\,\mathrm{m}$). Figure 12 depicts a comparison between the transient numerical velocity profiles $u=u(y,t)$ at the $x=\delta_x$ of the channel and the analytic solution (19) (convergence required, at most, one thousand terms in the series). It can be seen from this figure that the simulation results are fairly close to the exact solutions except for the initial transient stage (for example, $t=0.0005$). These differences, however, diminish with time. Moreover, agreement can be improved by using a finer mesh.

In order to test the second-order convergence of the ADBQUICKEST scheme when combined with the Crank–Nicolson implicit method, we consider the fully developed flow described above at $Re=500$ and simulation time $t=15$. Table III shows the convergence study in the L_1, L_2, and L_∞ norms. One can see from this table that second-order convergence rate is practically achieved

DOI: 10.1002/fld

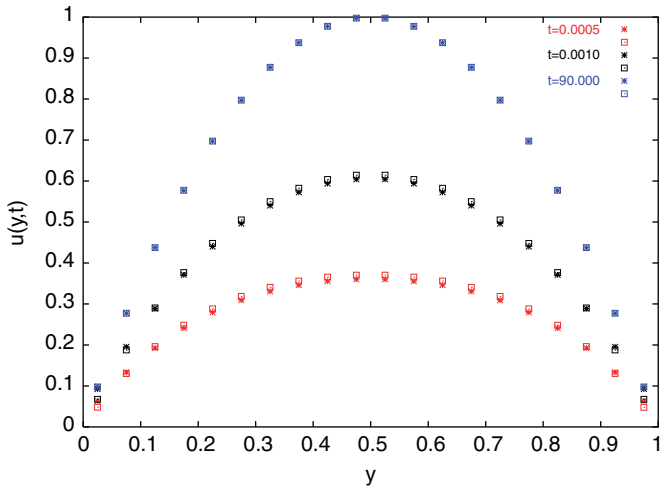

Figure 12. Comparison between numerical (stars) and analytic (squares) solutions for transient Poiseuille flow.

Table III. Convergence study of the ADBQUICKEST scheme, associated with the Crank–Nicolson method, as applied to the channel flow at $Re=500$ and output time $t=15$.

Mesh	L_1 error	L_1 order	L_2 error	L_2 order	L_∞ error	L_∞ order
100×20	1.4352e−3	—	1.1680e−3	—	1.9810e−3	—
200×40	2.6539e−4	1.975	2.9797e−4	1.970	5.5940e−4	1.824
400×80	6.6734e−5	1.992	7.4897e−5	1.992	1.4791e−4	1.919

when we used the combination of the ADBQUICKEST and Crank–Nicolson implicit schemes. A plausible explanation for the estimated convergence rate to be slightly below the expected value of 2 is that the hybrid (i.e. first-order upwind/CD) scheme is applied at cells adjacent to the rigid boundaries.

3.4.2. Jet plunging into a fluid at rest. This problem, an important early experiment by Taylor [41], consists of a jet flowing vertically into a box containing the same fluid at rest. The calculations were carried out using the axisymmetric GENSMAC code of Tomé *et al.* [42], which was appropriately modified to include the ADBQUICKEST scheme. With this new version of the code, we solved the full Navier–Stokes equations (14)–(16) with $\alpha=1$, $\eta(q)=1$, $\eta=\eta_0$ and $\beta=0$ (axisymmetric Newtonian case). The no-slip condition is applied on the box walls. Figure 13 displays two snapshots of this jet flow simulation and Taylor's experiment for $Re=200$. As one can see from this figure, there is qualitative agreement between the numerical results and the experiment of Taylor. In particular, in case (c) of this figure, the jet reaches the bottom forming an apparently toroidal structure. It is interesting to observe at this point that Tomé *et al.* [42, Figure 9, p. 458] also simulated this free surface flow by using second-order CD to approximate the advection terms: their numerical result, however, failed to capture this feature of the complicated flow structure.

DOI: 10.1002/fld

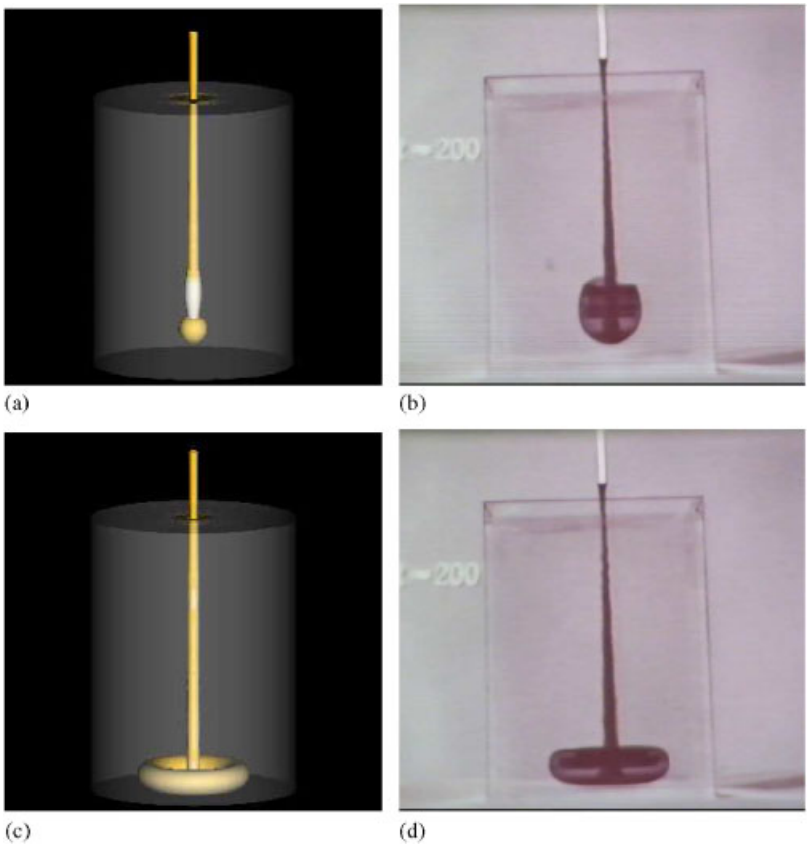

Figure 13. Jet plunging into a fluid at rest, using $Re=200$ and two different times: (a) 3D view of the numerical simulation at $t=40$; (b) Taylor's experiment; (c) 3D view of the numerical simulation at $t=100$; and (d) Taylor's experiment.

3.4.3. Generalized Newtonian fluid flow. Another important test is the flow of a generalized fluid in a straight pipe of circular cross section, radius $R=1.0\,\mathrm{m}$ and length $L=5R$, with entry and exit sections at $z=0.0$ and 10.0 m, respectively. The Reynolds number considered here is $Re=U_0R/\eta_0$, where U_0 is the averaged velocity, defined as the volumetric flow rate divided by the cross-sectional area, that is,

$$U_0=\frac{1}{\pi R^2}\int_0^{2\pi}\int_0^R v(r)r\,\mathrm{d}r\,\mathrm{d}\theta \tag{20}$$

The analytic solution $v=v(r)$ in Equation (20) is obtained by assuming that, in the z direction, the flow is completely developed and the pressure gradient is known. By applying these assumptions in dimensional form to Equations (14)–(16), with $\beta=1$ and $\eta(q)$ given by Equation (17) (axisymmetric generalized Newtonian case) and by imposing boundary conditions, axisymmetry at the center of

DOI: 10.1002/fld

the tube and no-slip velocity at the wall, we obtain

$$\frac{\partial}{\partial r}\left(\eta(q)\frac{\partial v}{\partial r}\right)+\frac{1}{r}\eta(q)\frac{\partial v}{\partial r}=\frac{\partial p}{\partial z},\quad \left.\frac{\partial v}{\partial r}\right|_{r=0}=0,\quad v|_{r=R}=0 \tag{21}$$

where, from the dimensional equation (18), $q=|\partial v/\partial r|$. This boundary value problem is solved as follows. Firstly, we solve the problem

$$\frac{\partial Z}{\partial r}+\frac{Z}{r}=\Delta p,\quad Z(0)=0 \tag{22}$$

where $Z=\eta(q)\partial v/\partial r$ and $\Delta p=\partial p/\partial z$. The solution of this initial value problem is $Z(r)=\Delta p/2r$. Secondly, with $\eta(q)$ given by the cross model, Equation (17), we solve the non-linear equation

$$\left[\eta_\infty+\frac{\eta_0-\eta_\infty}{1+\left(K\left|\dfrac{\partial v}{\partial r}\right|\right)^M}\right]\frac{\partial v}{\partial r}=Z(r) \tag{23}$$

for $\partial v/\partial r$. Finally, we solve the problem

$$\frac{\partial v}{\partial r}=f(r),\quad v(R)=0 \tag{24}$$

for $v(r)$, where $f(r)$ is an implicit solution of $\partial v/\partial r$ defined from Equation (21).

By considering, for instance, the pressure gradient $\Delta p=-0.50\,\mathrm{m/s^2}$ and the material parameters $M=0.50$, $\eta_0=1.820\,\mathrm{kg/(m\,s)}$, $\eta_\infty=0.00\,\mathrm{kg/(m\,s)}$, and $K=1.5\,\mathrm{s}$, we derive, using MAPLE® software, the following analytic velocity vector field $\mathbf{u}=(0,v(r))^{\mathrm{T}}$, with $v(r)$ given by

$$\begin{aligned}v(r)=&-0.0686813187r^2-0.004717123533r^3-0.000544686509r^2(r(75r+1456))^{1/2}\\&-0.002643545188r(r(75r+1456))^{1/2}+0.07698003595(r(75r+1456))^{1/2}\\&-6.471111116ln(8.66025404r+84.0621992+(r(75r+1456))^{1/2})\\&+28.77589119\end{aligned} \tag{25}$$

Integrating Equation (20), with $v(r)$ given by Equation (25), we obtain the desirable input velocity scale as $U_0=0.05131576119\,\mathrm{m/s}$. Once again, the calculations were carried out using the GENSMAC code [42], appropriately modified to include the ADBQUICKEST scheme.

The numerical solutions corresponding to four different uniform meshes consisting of 5×25 ($\delta r=\delta z=0.2\,\mathrm{m}$) , 10×50 ($\delta r=\delta z=0.1\,\mathrm{m}$) , 20×100 ($\delta r=\delta z=0.05\,\mathrm{m}$) , and 40×200 ($\delta r=\delta z=0.025\,\mathrm{m}$) computational cells in the (r,z) directions are compared at the non-dimensional time $t=30$. The numerical results for these four meshes have been obtained by imposing, at the inflow boundary, the analytic velocity profile (Equation (25)) (plane and parabolic profiles were also employed yielding similar results, but the CPU time increased considerably).

Figure 14 depicts comparisons, at the cross-section given by $z=0.50\,\mathrm{m}$, of the non-dimensional velocity profile $v=v(r)$ obtained on these meshes together with the non-dimensional non-Newtonian analytic solution (Equation (25)). In this figure, for simple comparison, the Newtonian

DOI: 10.1002/fld

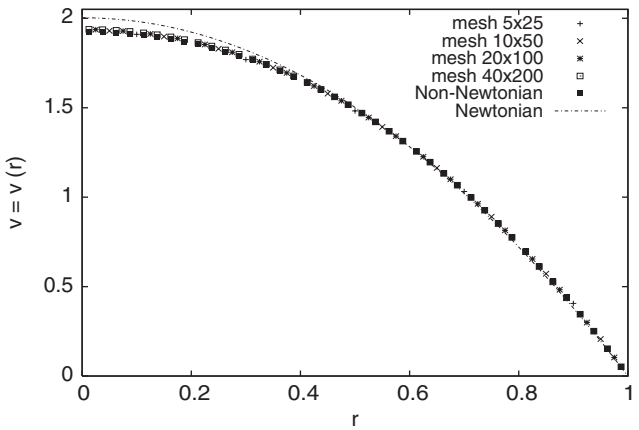

Figure 14. A comparison between of the numerical solutions, on four different grids, and the Newtonian and generalized Newtonian analytic solutions.

Table IV. Normalized L_1 errors in the v velocity.

Mesh	L_1 error
5×25	0.01107202080
10×50	0.00348490517
20×100	0.00347384717
40×200	0.00340860191

analytic solution is also presented. From this figure, it is seen that, during grid and time-step refinement, little change in the numerical $v = v(r)$ profiles is observed, indicating convergence of the numerical solution on four meshes. Furthermore, the results obtained with the present numerical procedure are in good agreement with the derived generalized Newtonian analytic solution (Equation (25)).

A more quantitative assessment of the level of agreement between the calculated solutions on the four meshes and the generalized Newtonian theoretical solution (Equation (25)) can be obtained by looking at the normalized error in the L_1 norm. This is summarized in Table IV. These results quantify the observations regarding Figure 14. In particular, the numerical solution on the fine mesh, 40×200 computational cells, shows a very small error.

Figures 15 and 16 display the non-dimensional numerical solutions on the 40×200 mesh and analytic results for the deformation rate and viscosity, respectively. These figures illustrate that the computational simulation using the ADBQUICKEST scheme accurately represents the behavior of the generalized Newtonian fluid flow in a circular pipe.

3.4.4. Application: direct computation of the collapse of fluid columns. Collapse of fluid columns (or dam-break flows) are an important practical problem in civil engineering and their prediction is a required element in the design of a dam and its surrounding environment [43]. This free surface flow problem was first studied experimentally by Martin and Moyce [44] and then used as a test bed by developers of the volume-of-fluid (VOF)-based numerical methods (see, for instance,

DOI: 10.1002/fld

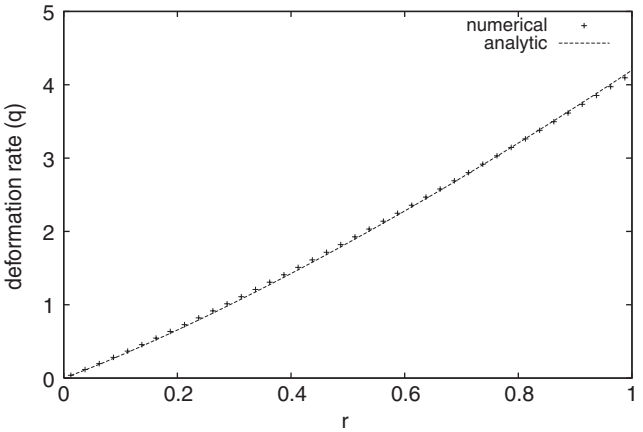

Figure 15. Behavior of the deformation rate versus radial distance for the numerical and the analytic solution.

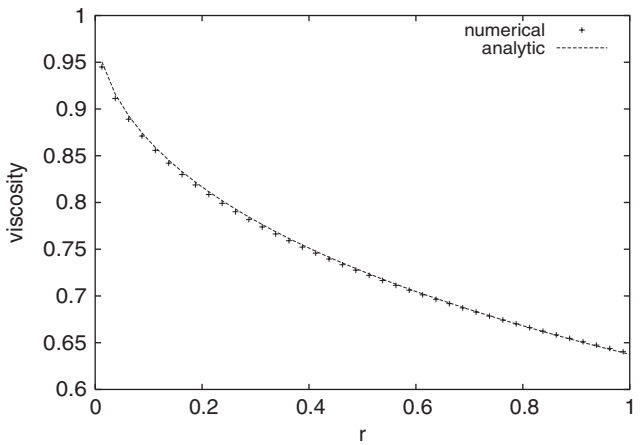

Figure 16. Behavior of the viscosity versus radial distance for the numerical and the analytic solutions.

[45, 46]). Later, Koshizuka and Oka [47] repeated the experiment and used it to check their moving-particle semi-implicit code. Since then, this problem has been investigated numerically by various researchers (see, for example, [48]), as a benchmark test for free surface flow numerical methods. Recently, Violeau and Issa [49] used this problem to check the performance of their gridless smoothed particle hydrodynamics κ–ε turbulence model.

By using the ADBQUICKEST scheme implemented into the 2D and 3D versions of the Freeflow Navier–Stokes flow solver of Castelo *et al.* [40], we performed a direct numerical simulation of this unsteady free surface flow. For this we add, in Equation (15), the gravitational contribution g_z/Fr^2, where $Fr = U/\sqrt{L|\mathbf{g}|}$ is the Froude number. The problem is described as follows.

A rectangular fluid column of $a = 0.10\,\mathrm{m}$ wide and $b = 0.050\,\mathrm{m}$ high (and in the 3D case a fluid block of $b = 0.05\,\mathrm{m}$ length, $a = 2b$ wide and $c = 2b$ high) in hydrostatic equilibrium is

DOI: 10.1002/fld

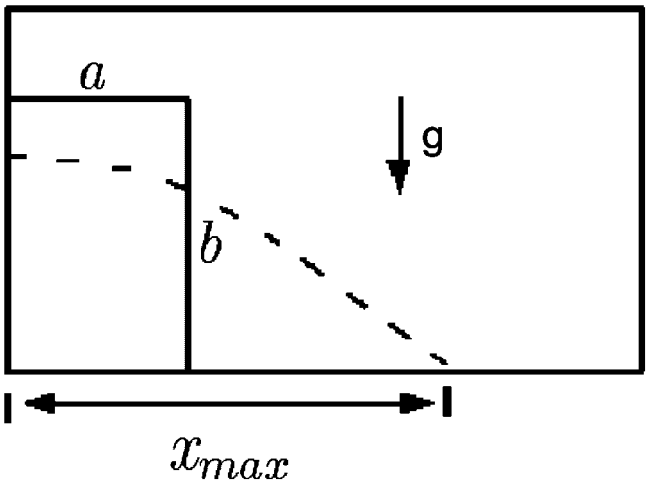

Figure 17. Schematic illustration for a 2D collapse of a fluid column.

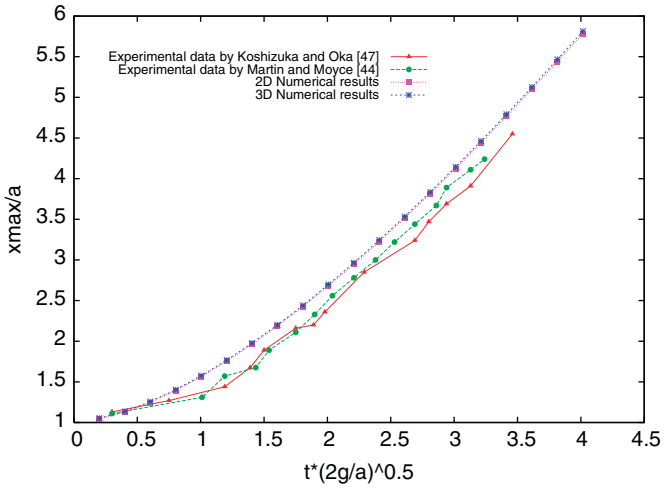

Figure 18. Computations and experimental data for the surge front position $x_{\max}$.

confined between walls. At the beginning, a wall is instantaneously removed and the fluid is subject to vertical gravity and is free to flow out along a rigid horizontal wall. Figure 17 depicts this problem in the 2D case. The Reynolds number based on the characteristic length $L=b$ and the characteristic velocity $U=\sqrt{L|\mathbf{g}|}$ is $Re=LU/\nu=99045.444$ ($|\mathbf{g}|=9.81\,\mathrm{ms}^{-2}$). The meshes used for this problem were 150×75 ($\delta_x=\delta_y=0.002\,\mathrm{m}$) computational cells in the 2D case and $150\times50\times75$ ($\delta_x=\delta_y=\delta_z=0.002\,\mathrm{m}$) computational cells in the 3D case. The motion of the fluid front position $x_{\max}$ versus time, obtained by the 2D and 3D numerical results, was compared with the experimental data of Koshizuka and Oka [47] and Martin and Moyce [44] in Figure 18. As shown in this figure, both 2D and 3D calculations agree fairly well with the experimental data,

DOI: 10.1002/fld

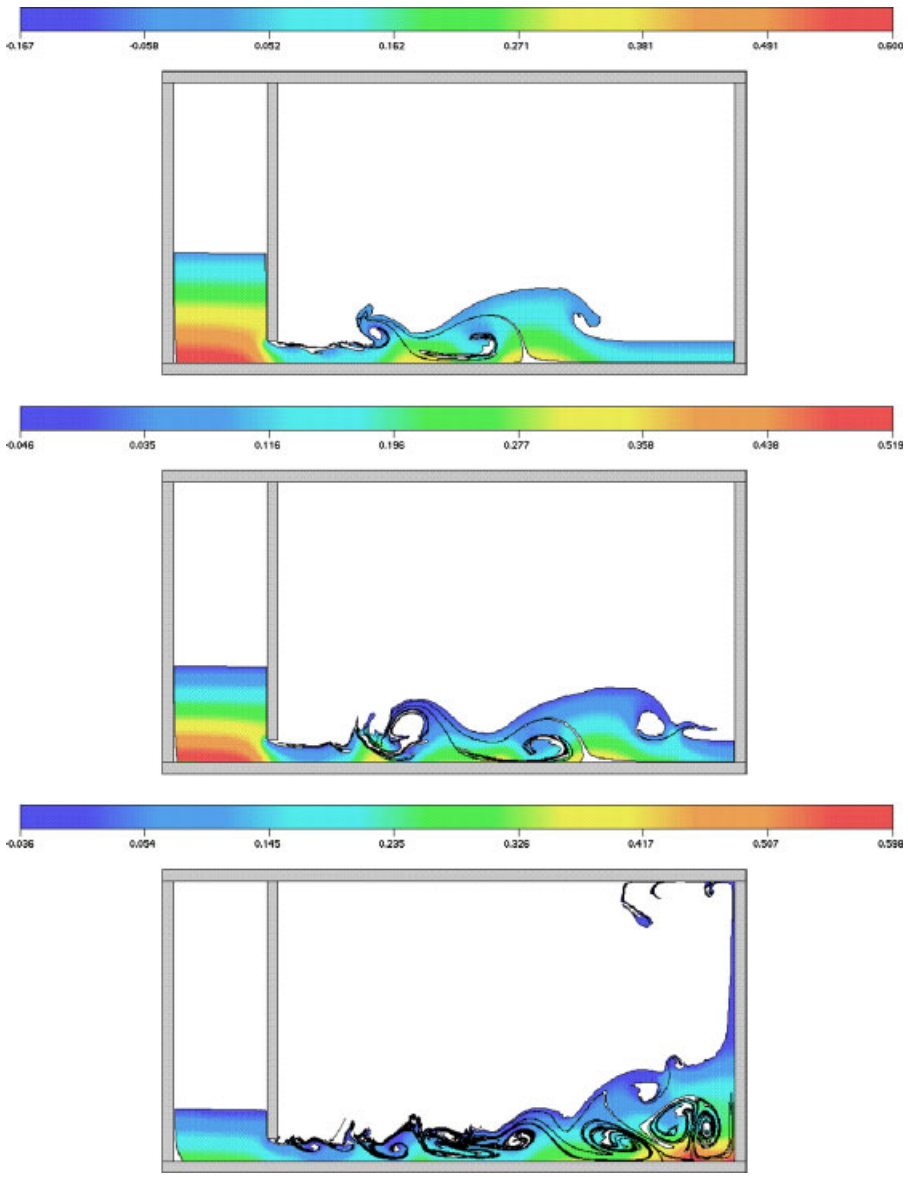

Figure 19. Non-dimensional time evolution of the non-dimensional pressure contours and free surface deformation of a 2D numerical simulation of the partial opening of a sluice gate.

specially in the comparison with the results of Martin and Moyce, providing confidence in the numerical solutions.

We conclude this paper by presenting the numerical simulation of another type of dam break flow (see [50]), which corresponds to a strong free surface motion generated by a sluice gate. This problem is generally used as a model to study flows in hydraulic structures, where the effects of the

DOI: 10.1002/fld

free surface, turbulence fluctuations and pressure distribution are usually required to be determined (see [51, 52]). The parameters employed in our simulation are the same as that for the collapse of fluid column. The development of non-dimensional pressure distributions, together with the free surface deformation at three non-dimensional times, are presented in Figure 19. One can see from this figure that there is a visible transition to turbulence, at least occurring at scales greater than the discretization scale.

4. CONCLUSIONS

The high-order upwind ADBQUICKEST finite difference scheme has been successfully used to solve a variety of complicated advection–diffusion problems, containing discontinuities and complex structures, namely advection of scalars, shock tube problems, 2D Newtonian flow, axisymmetric Newtonian/generalized Newtonian flows, and a 3D free surface flow.

The numerical results obtained with the ADBQUICKEST scheme complement those found in Ferreira *et al.* [16] and confirm the capability of this high-order upwind scheme to control the generation of unphysical oscillations in the vicinity of discontinuities.

It is intended that future research will consider: (a) extension of the study to 2D Burgers equation, 2D shock tube problems, and (b) an investigation of the performance of the ADBQUICKEST scheme for solving 3D turbulent and non-Newtonian incompressible free surface flows. These should provide a severe test for any high-order upwinding scheme.

ACKNOWLEDGEMENTS

We gratefully acknowledge the support provided by *FAPESP* (Grants 03/12612-9, 04/16064-9, 05/51458-0 and 06/05910-1) and *CNPq* (Grants 304201/2005-7 and 472030/2006-0). We are also grateful to the anonymous referees for their valuable comments to improve the paper.

REFERENCES

1. Fletcher CAJ. *Computational Techniques for Fluid Dynamics*. Springer: Berlin, 1991.
2. Gentry RA, Martin RE, Daly BJ. An Eulerian differencing method for unsteady compressible flow problems. *Journal of Computational Physics* 1966; **8**:55–76.
3. Leonard BP. Universal limiter for transient interpolation modeling of the advective transport equations: the ULTIMATE conservative difference scheme. *NASA Technical Memorandum 100916*, *ICOMP-88-11*, 1988.
4. Spalding DB. A novel finite difference formulation for differential expressions involving both first and second derivatives. *International Journal for Numerical Methods in Fluids* 1972; **4**:551–559.
5. Huh KY, Golay MW, Manno VP. A method for reduction of numerical diffusion in the donor cell treatment of convection. *Journal of Computational Physics* 1986; **83**:201–221.
6. LeVeque RJ. *Numerical Methods for Conservation Laws*. Lectures in Mathematics. Birkhauser: Basel, 1990; 214.
7. Shyy W. A study of finite difference approximations to steady-state, a convection-dominated flow problem. *Journal of Computational Physics* 1985; **57**:415–438.
8. Leonard BP. A stable and accurate modelling procedure based on quadratic interpolation. *Computer Methods in Applied Mechanics and Engineering* 1979; **19**:59–98.
9. Lax PD, Wendroff B. Systems of conservations laws. *Communications on Pure and Applied Mathematics* 1960; **13**:217–237.
10. Pierce CD. Progress-variable approach for large-eddy simulation of turbulence combustion. *Ph.D. Thesis*, Stanford University, 2001.
11. Varonos A, Bergeles G. Development and assessment of a variable-order non-oscillatory scheme for convection term discretization. *International Journal for Numerical Methods in Fluids* 1998; **26**:1–16.

DOI: 10.1002/fld

12. Zhu J. On the higher-order bounded discretization schemes for finite volume computations of incompressible flows. *Computer Methods in Applied Mechanics and Engineering* 1992; **98**:345–360.
13. Gaskell PH, Lau AKC. Curvature-compensated convective transport: SMART, a new boundedness-preserving transport algorithm. *International Journal for Numerical Methods in Fluids* 1988; **8**:617–641.
14. Song B, Liu GR, Lam KY, Amano RS. On a higher-order bounded discretization scheme. *International Journal for Numerical Methods in Fluids* 2000; **32**:881–897.
15. Alves MA, Oliveira PJ, Pinho FT. A convergent and universally bounded interpolation scheme for the treatment of advection. *International Journal for Numerical Methods in Fluids* 2003; **41**:47–75.
16. Ferreira VG, Oishi CM, Kurokawa FA, Kaibara MK, Cuminato JA, Castelo A, Mangiavacchi N, Tomé MF, McKee S. A combination of implicit and adaptative upwind tools for the numerical solution of incompressible free surface flows. *Communications in Numerical Methods in Engineering* 2007; **23**:419–445.
17. Kaibara MK, Ferreira VG, Navarro HA, Cuminato JA, Castelo AF, Tomé MF. Upwind schemes for convection dominated problems. *Proceedings of the 18th International Congress of Mechanical Engineering*, Ouro Preto, MG, Brazil, 2005.
18. Leonard BP. Simple high-accuracy resolution program for convective modeling of discontinuities. *International Journal for Numerical Methods in Engineering* 1988; **8**:1291–1318.
19. Leonard BP, Niknafs H. Sharp monotonic resolution of discontinuities without clipping of narrow extrema. *Computers and Fluids* 1991; **19**:141–154.
20. Waterson NP, Deconinck H. Design principles for bounded higher-order convection schemes—a unified approach. *Journal of Computational Physics* 2007; **224**:182–207.
21. Harten A. On a class of high resolution total-variation-stable finite-difference schemes. *SIAM Journal on Numerical Analysis* 1984; **21**:1–23.
22. Sweby PK. High resolution schemes using flux limiters for hyperbolic conservation laws. *SIAM Journal on Numerical Analysis* 1984; **21**:995–1011.
23. Harten A. ENO scheme with subcell resolution. *Journal of Computational Physics* 1989; **83**:148–184.
24. Titarev VA, Toro EF. WENO schemes based on upwind and centred TVD fluxes. *Computers and Fluids* 2005; **34**:705–720.
25. Herrmann M, Blanquart G, Raman V. Flux corrected finite volume scheme for preserving scalar boundedness in reacting large-eddy simulations. *AIAA Journal* 2006; **44**:2879–2886.
26. Balsara DS, Shu C-W. Monotonicity preserving weighted essentially non-oscillatory schemes with increasingly high order of accuracy. *Journal of Computational Physics* 2000; **160**:405–452.
27. Rogerson A, Melberg E. A numerical study of the convergence properties of ENO schemes. *Journal of Scientific Computing* 1994; **18**:555.
28. Wei GW, Gu Y. Conjugated filter approach for solving Burger's equation. *Journal of Computational and Applied Mathematics* 2002; **149**:439–456.
29. Toro EF. *Riemann Solvers and Numerical Methods for Fluid Dynamics*, *A Practical Introduction* (2nd edn). Springer: Berlin, 1991.
30. Karpman VI. *Non-linear Waves in Dispersive Media*. Fluid Mechanics. Pergamon: Elmsford, New York, NY, 1975.
31. Roe PL. Characteristic-based schemes for the Euler equations. *Annual Review of Fluid Mechanics* 1986; **18**: 337–365.
32. Yang H. An artificial compression method for ENO schemes: the slope modification method. *Journal of Computational Physics* 1990; **89**:125–160.
33. Shu C-W, Osher S. Efficient implementation of essentially non-oscillatory shock capturing schemes, II. *Journal of Computational Physics* 1989; **83**:32.
34. Billet G, Louedin O. Adaptive limiters for improving the accuracy of the MUSCL approach for unsteady flows. *Journal of Computational Physics* 2001; **170**:161–183.
35. Levy D, Puppo G, Russo G. A fourth-order central WENO scheme for multidimensional hyperbolic systems of conservation laws. *SIAM Journal on Scientific Computing* 1991; **24**:480–506.
36. Cross MM. Rheology of non-Newtonian fluids: a new flow equation for pseudo-plastic systems. *Journal of Colloid Science* 1965; **20**:417–437.
37. Bird RB, Armstrong RC, Hassager O. *Dynamics of Polymeric Liquids* (2nd edn). Fluid Mechanics, vol. I. Wiley: New York, 1987.
38. Morris JP, Fox PJ, Zhu Y. Modeling low Reynolds number incompressible flows using SPH. *Journal of Computational Physics* 1997; 214–226.

DOI: 10.1002/fld

39. Takemitsu N. Finite difference method to solve incompressible fluid flow. *Journal of Computational Physics* 1985; **61**:499–518.
40. Castelo A, Tomé MF, Cesar ML, Cuminato JA, McKee S. Freeflow: an integrated simulation system for three-dimensional free surface flows. *Journal of Computers and Visualization in Science* 2000; **2**:199–210.
41. Taylor GI. Low-Reynolds number flows. *National Committee for Fluid Mechanics Films. Illustrated Experiments in Fluid Mechanics* (2nd edn), U.S.A., 1974; 47–54. ISBN: 0-262-14014-4.
42. Tomé MF, Castelo A, Murakami J, Cuminato JA, Minghim R, Oliveira MCF, Mangiavacchi N, McKee S. Numerical simulation of axisymmetric free surface flows. *Journal of Computational Physics* 2000; **157**:441–472.
43. Ataie-Ashtiani B, Farhadi L. A stable moving-particle semi-implicit method for free surface flows. *Fluid Dynamics Research* 2006; **38**:241–256.
44. Martin JC, Moyce WJ. An experimental study of the collapse of liquid columns on a rigid horizontal plate. *Philosophical Transactions of the Royal Society of London*, *Series A*: *Mathematical*, *Physical and Engineering Sciences* 1952; **244**:312–324.
45. Hirt CW, Nichols BD. Volume of fluid (VOF) method for the dynamics of free boundaries. *Journal of Computational Physics* 1983; **8**:284–294.
46. Kim MS, Lee WI. A new VOF-based numerical scheme for the simulation of fluid flow with free surface. Part I: new free surface-tracking algorithm and its verification. *International Journal for Numerical Methods in Fluids* 2003; **42**:765–790.
47. Koshizuka S, Oka S. Moving-particle semi-implicit method for fragmentation of incompressible fluids. *Nuclear Science and Engineering* 1996; **123**:421–434.
48. Greaves DM. Simulation of viscous water column collapse using adapting hierarchical grids. *International Journal for Numerical Methods in Fluids* 2006; **50**:693–711.
49. Violeau D, Issa R. Numerical modelling of complex turbulent free-surface flows with the SPH method: an overview. *International Journal for Numerical Methods in Fluids* 2007; **53**:277–304.
50. Harlow FH, Welch E. Numerical calculation of time-dependent viscous incompressible flow of fluid with free surface. *Physics of Fluids* 1965; **8**:2182–2189.
51. Mouaze D, Murzyn F, Chaplin JR. Free surface length scale estimation in hydraulics jumps. *Journal of Fluids Engineering* 2005; **127**:1191–1193.
52. Sankaranarayanan S, Suresh Rao H. Finite element analysis of free surface flow through gates. *International Journal for Numerical Methods in Fluids* 1996; **22**:375–392.

DOI: 10.1002/fld